Development of an extended reactor configuration to analyze preferential segregation impact on spray autoignition

Zakaria Bouali, J. Reveillon, Cécile Pera

Version of Record: https://www.sciencedirect.com/science/article/pii/S0016236121007468
Manuscript_afc2963bb23c2e84cbdf4c20d9936f63

Development of an extended reactor configuration to analyze preferential segregation impact on spray autoignition

Z. Bouali [a,b,*], J. Reveillon[c], C. Pera[b,d]

[a] *Institut Pprime, UPR3346 CNRS - ENSMA and University of Poitiers - BP40109 - 86961, Poitiers, France*
[b] *IFP Energies nouvelles, 1-4 avenue de Bois-Préau, 92500 Rueil-Malmaison, France*
[c] *CORIA, University and INSA of Rouen, Avenue de l'Université, 76800 St Etienne du Rouvray France*
[d] *OROVEL Ltd*

Abstract

The chemical reactor concept, usually based on a homogeneous mixture, is extended to non-homogeneous two-phase flows to study the impact of preferential segregation on the autoignition of an n-heptane spray in air. To introduce inhomogeneities, two-dimensional reactors are resolved thanks to direct numerical simulations (DNS) with Eulerian/Lagrangian description to follow the evolution of the carrier phase and the dispersed evaporating droplets, respectively. Two-way coupling is considered through exchange of mass, momentum, and energy between the carrier-gas phase and the dispersed phase. A chemistry mechanism with 29 species and 52 reactions was chosen to describe the chemical reaction paths. Several simulations were performed with various initial gas temperatures (i.e. low, intermediate and high) and various geometrical and physical characteristics of the preferential segregation. Results confirmed that evaporative cooling, vapor mass quantity and turbulence mixing play important roles in the two-phase flow autoignition. We discussed the ignition delay as well as the

*Corresponding author
Email address: zakaria.bouali@ensma.fr (Z. Bouali)

Nomenclature

$()^{st}$	Stoichiometric value	S_L	Segregation level
$()_0$	Initial values	T_0	Initial gas temperature
$()_k$	Droplet properties	Y_v	Fuel vapor mass fraction
$()_\alpha$	Properties of α^{th} species	Y_α	Mass fraction of α^{th} species
δ_c	Characteristic cluster size	Z	Mixture fraction
$\overline{\xi^2}$	Density variance	Z_{MR}	Most reactive mixture fraction
$\overline{\xi}$	Mean spray density	0D	Zero-dimensional
ξ	Local density of spray	2D	Two-dimensional
a_0	Initial diameter of droplets	3D	Three-dimensional
a_k	droplet diameter	DNS	Direct numerical simulation
$B_{m,k}$	Mass transfer coefficient of k^{th} droplet	HT	High temperature
$B_{T,k}$	Heat transfer coefficient of k^{th} droplet	IT	Intermediate temperature
NTC	Negative Temperature Coefficient	LT	Low temperature
		PDF	Probability density functions

location of the first hot spots according to the initial gas temperatures. The dependence of most reactive mixture fraction on initial carrier-gas temperature is non-monotonic, thus there is a strong correlation between the first autoignition location and low scalar dissipation rate. On the other hand, the autoignition can start whatever the vorticity magnitude is.

Keywords: `autoignition`, two-phase flows, evaporation, preferential segregation, NTC, DNS

1. Introduction

During the last decades, combustion chamber modeling has been extensively developed thanks to better understanding in various physical phenomena interacting in engines from the liquid fuel injection, down to combustion processes and gas exhaust. However, for their environmentally and economically optimisation, model accuracy still needs to be improved. Many physical and chemical phenomena interact within the chamber. Pollutant formation directly depends on the combustion which itself depends on the mixing quality and local thermodynamic conditions. After primary atomization close to the injector tip, a secondary atomization generates a dispersed spray. These droplets are small enough to undergo the turbulent velocity fluctuations and they evaporate according to the local flow properties (temperature, pressure, fuel's vapor concentration). Modern direct injection engines now use multiple split-injections that can even overlap each other (a spray can be injected while the previous one is still not completely dispersed or has started to autoignite). From a modeling point of view, it is necessary to correctly represent ignition while mixing and droplet evaporation still occur.

Nowadays, optimization of direct injection car engines have lead to a strong increase of the injection pressure and all engine cycles are so accurately cadenced that they generally overlap each other. Thus, when ignition occurs, mixing and evaporation processes are mostly still in progress. Depending on mixing and evaporation, ignition delay defines the combustion regimes and the structure of the resulting flames.

Previous numerical works on the autoignition in single-phase flows have revealed that ignition occurs first in regions of the flow characterized by: (i) a well-defined value of mixture fraction named "most reactive mixture fraction" and (ii) a low scalar dissipation rate. This result was obtained with two-dimensional

(2D) DNS of Homogeneous Isotropic Turbulence (HIT) considering a simplified chemistry model [1]. It was later confirmed by other studies including three-dimensional (3D) effects [2], more complex flow [3] and/or complex chemistry [4]. Viggiano [4] highlighted the importance of taking into account at least a skeletal chemistry mechanism to properly predict the ignition. Using a chemistry for hydrogen-air, the effect of temperature heterogeneity as well as detailed chemical paths on the autoignition was investigated by [5]. They numerically study the effects of different temperature distributions on the autoignition of a turbulent homogeneous mixture. They found that the presence of a hot core gas leads to an increase in burn duration, while a cold core gas may lead to an undesirable slow combustion of the end gas. It is important to emphasize that this temperature variation topic is omnipresent in the framework of two-phase combustion. However, even if gaseous flow investigations offer major ground knowledge, there are numerous issues that lack answers. And it has been only very recently that research teams were able to tackle some of them. Despite the large number of papers dedicated to single-phase flows [6], considerably less studies were devoted to spray autoignition. These last ones adopt, in general, a coupling of the formalism DNS for carrier phase with the particle-source in cell model for dispersed phase. The autoignition of n-heptane sprays at high temperature was investigated numerically by Wang and Rutland [7, 8] considering a 2D configuration and a skeletal mechanism of n-heptane. They found that an increase of the initial gas temperature leads to a decrease of the autoignition delay, while an opposite behavior was observed for the global equivalence ratio. The impact of initial droplet size on the autoignition location was investigated by Schroll et al. [9] using three-dimensional DNS with one-step global chemistry. They performed three simulations with the same initial global equivalence ratio but different initial droplet size. They found that the initial droplet size strongly

impacts the autoignition delay but does not affect the value of the most reactive mixture fraction. Thereafter, 3D-DNS with detailed chemistry were performed to investigate the impact of spray properties, the turbulence intensity and shear on the ignition. Borghesi et al. [10] have been analyzed the effect of the initial turbulence in the carrier gas, the global equivalence ratio in the spray region and the initial droplet size distribution of the spray autoignition. Their results revealed that (i) turbulence reduces the ignition delay time as it promotes mixing between air and fuel vapor, (ii) a larger number of ignition kernels is directly related to high values of global equivalence ratio, due to higher probability of the most reactive regions, and (iii) spray polydispersity results in the occurrence of ignition over a wider range of mixture fraction values. The impact of shear on evaporation and spray autoignition process was analyzed by Abdelsamie et al. [11]. They found that the autoignition delay time strongly depends on the droplet diameter and the jet velocity, while it is far less sensitive onto the equivalence ratio. They observed also that with high shear, ignition occurs on the lean side, and peak heat release is found near stoichiometry in a premixed combustion mode. In the absence of shear, ignition occurs simultaneously over a broad range of mixture fractions, and peak heat release is found for a rich mixture involving both premixed and non-premixed flames. In spark ignition context, Neophytou et al. [12, 13] attest that the success of ignition was linked to the number of droplets engulfed by the spark. They observed a strong dependence of the reactive processes with the spray properties. It appears that the heat release rate is lower than in the equivalent gaseous problem and is limited by the evaporation rate. They also observed a large scatter of heat release and species in mixture fraction space making difficult the development of adapted combustion models.

Despite the aforementioned researches, there are numerous issues concerning

autoignition in sprays that lack answers, particularly in the low and intermediate temperature range where *cool flame* and Negative Temperature Coefficient (NTC, i.e. autoignition delay increases with temperature) phenomena take place.

This issue has been studied by 2D-DNS considering detailed chemistry in purely gaseous context. The influence of variations in the initial temperature and the ratio of turbulence to ignition delay timescale on multi-stage ignition of a lean n-heptane/air mixture was studied by Yoo et al. [14]. They observe that, (i) regardless of the mean initial temperature, the mean heat release rate increases more slowly with increasing thermal stratification and (ii) ignition delay decreases with increasing thermal stratification for high mean initial temperature relative to the NTC regime. It is, however, increased with increasing thermal fluctuations for relatively low mean initial temperature resulting from a longer overall ignition delay of the mixture. More recently, Krisman et al. [15] have been studied the behavior of the low-temperature chemistry and its influences on the high-temperature ignition. They have discussed the location of first-stage autoignition and highlighted its impact on the second-stage autoignition delay.

Conversely, studies dedicated to autoignition at low and intermediate temperature in two-phase context was limited to: (i) a non-dimensional homogeneous reactor [16] or (ii) one isolated droplet one-dimensional configurations [17, 18] and even if there are still unaddressed issues in these basic configurations, the dispersing nature of the spray and the preferential segregation effects lead to other difficulties and to combustion regimes that could not be characterized. Indeed, as described by Aggarwal [19] from a qualitative point of view, there are three dominant ignition modes and corresponding ignition delays: droplet ignition, group ignition and spray ignition. First, similarly to the

combustion regimes described by Chiu et al. [20, 21], ignition can occur either individually for droplets separated by a wide interspace, or around clouds of droplets if they are too close to each other to allow for diffusion of heat inside the cloud. A third mode: the spray ignition mode, considers a global ignition of the spray for droplets close to each other but surrounded by a hot atmosphere. In the context of internal combustion engine, where droplets are dispersed in a hot environment, this last mode is of particular interest. Usual homogeneous reactor studies offer better insights of the impacts of a liquid phase onto ignition properties but they cannot display any geometrical aspect of the spray dispersion since there is no spatial information. However, in practical systems, preferential segregation of droplets early appears because of strong turbulent mixing [22]. It leads to the formation of non-homogeneous pockets of fuel vapor that cannot be characterized by non-dimensional approaches though there is a direct impact on combustion regimes and model performances.

The objective of the present work is to use direct numerical simulation associated with a Lagrangian dispersed phase solver (DNS-DPS) to:

(i) extend homogeneous reactors studies to multiple clouds or clusters systems, the size and droplet density of which are prescribed. It allows accounting for the geometrical aspect of the spray in addition to the fundamental thermodynamical properties.

(ii) take into account the effect of preferential segregation of droplets on autoignition and various ignition shell.

The segregation is defined by the spray density variance and the characteristic size of the clouds (or clusters) of droplets. Of course, three-dimensional computations would have been better, however, computational's costs would have been skyrocketing to simulate large enough configurations to carry out accurate statistics (statistics need multiple integral length scales performed over long

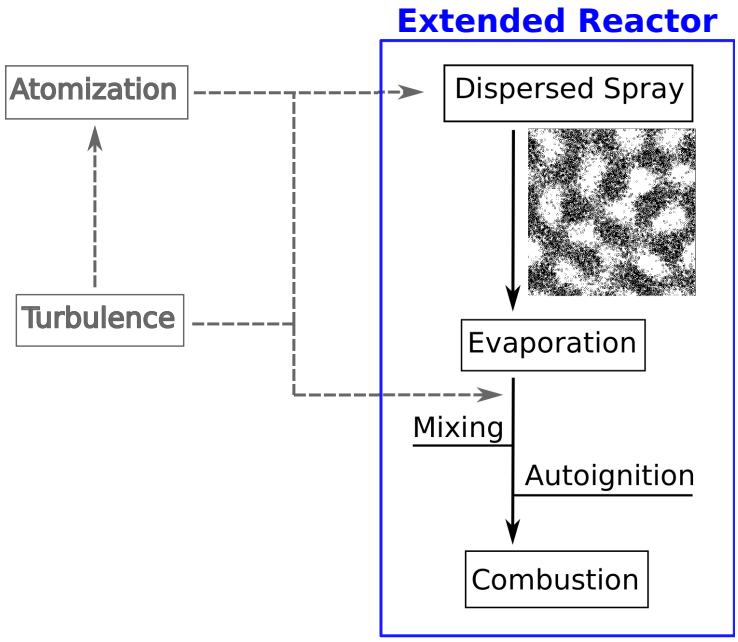

Figure 1: Phenomena taken into account by the Extended Reactor (ER).

enough rotating turbulent times). However, as underlined by Wang and Rutland [8] and shown by Sreedhara and Lakshmisha [2], the topology of autoignition spots remains similar enough irrespective of whether the flow is represented in two or three dimensions. It remains a technical challenge that still need to be addressed if a wide range of droplet clouds have to be considered. As a first step, one wishes to separate mixing and turbulence effects from the spray topology. Therefore, the droplets are first embedded in a quiescent atmosphere although convection due to gas dilatation is characterized. This 'Extended Reactor' (ER) configuration must be considered as a 2D (or 3D) extension of a usual non-dimensional reactor that is not able to consider spray preferential segregation. Figure 1 summarize the physical phenomena involved or that can be involved in our ER. This multiple dimension reactor involved, at least, phenomena outlined in blue color and can also integrate the effect of the turbulence and the atomization.

2. Physical model and configuration

2.1. Physical model

All simulations have been performed with the DNS code `Asphodele` [23, 24]. This reactive solver consider an Eulerian description of the gas coupled to a Lagrangian description of the liquid phase. The coupling between both phases is achieved thanks to the introduction of source terms in the mass, momentum, and energy equations for the continuous gas phase, while the effects of the gas phase are introduced in the form of boundary conditions applied at the boundary layer (gas film) surrounding the droplets.

The evolution of the droplet diameter and temperature are derived from the quasi-steady isolated droplet models, while the evolution of droplet velocity and position are derived from the drag model. By denoting $\mathbf{v}_k$ and $\mathbf{x}_k$ the velocity and position vectors of the k^{th} droplet, the following set of expressions:

$$\frac{d\mathbf{x}_k}{dt} = \mathbf{v}_k \tag{1}$$

$$\frac{d\mathbf{v}_k}{dt} = \frac{1}{\mathcal{T}_{\mathrm{v},k}}\left(\mathbf{u}\left(\mathbf{x}_k,t\right)-\mathbf{v}_k\right) \tag{2}$$

$$\frac{da_k^2}{dt} = -\frac{a_k^2}{\mathcal{T}_{a,k}} \tag{3}$$

$$\frac{dT_k}{dt} = \frac{1}{\mathcal{T}_{T,k}}\left(T(\mathbf{x}_k,t)-T_k-\frac{B_{T,k}L_v}{C_p}\right) \tag{4}$$

are used to track droplet evolution in the computational domain. The scalar $T(\mathbf{x}_k,t)$ and the vector $\mathbf{u}\left(\mathbf{x}_k,t\right)$ represent the gas temperature and the gas velocity at the droplet position $\mathbf{x}_k$. a_k is the diameter of k^{th} droplet, L_v the latent heat of evaporation and C_p the heat capacity of the surrounding gas mixture. The quantities $\mathcal{T}_{\mathrm{v},k}$, $\mathcal{T}_{a,k}$, and $\mathcal{T}_{T,k}$ represent kinetic, evaporation, and

heat relaxation time scales:

$$\mathcal{T}_{\mathrm{v},k} = \frac{\rho_l a_k^2}{18 C_{D,k} \mu} \tag{5}$$

$$\mathcal{T}_{a,k} = \frac{S_c}{4 Sh_c} \frac{\rho_l}{\mu} \frac{a_k^2}{\ln(1+B_{m,k})} \tag{6}$$

$$\mathcal{T}_{T,k} = \frac{P_r}{6 Nu_c} \frac{C_l}{C_p} \frac{\rho_l a_k^2}{\mu} \frac{B_{T,k}}{\ln(1+B_{T,k})} \tag{7}$$

where ρ_l, C_l are the density and heat capacity of the liquid. μ is the gas viscosity, S_c and P_r are the Schmidt and Prandtl numbers and Sh_c and Nu_c denote the convective Sherwood and Nusselt numbers, respectively. The quantities $B_{m,k}$ and $B_{T,k}$ represent the mass and heat transfer numbers (Spalding numbers) of k^{th} droplet. $B_{m,k} = (Y_v^s - Y_v)/(1 - Y_v^s)$ corresponds to the normalized mass flux of fuel vapor from the droplet surface Y_v^s to the surrounding gas Y_v. Its temperature counterpart is $B_{T,k} = (B_{m,k}+1)^{Pr/Sc.Sh_c/Nu_c} - 1$. For more information, see [25].

The resolution of the reactive multi-species carrier gas phase is based on the standard set of conservation equations within the low Mach number approximation. Equations are considered for the mass (i.e., density of the mixture ρ), momentum components (ρu_i), mass fraction of each chemical species (Y_α), and sensible enthalpy.

$$\frac{\partial \rho}{\partial t} + \frac{\partial \rho u_i}{\partial x_i} = \dot{m} \tag{8}$$

$$\frac{\partial \rho u_i}{\partial t} + \frac{\partial \rho u_i u_j}{\partial x_j} = -\frac{\partial p_1}{\partial x_i} + \frac{\partial \tau_{ij}}{\partial x_j} + \dot{\mathrm{v}}_i \tag{9}$$

$$\frac{\partial \rho Y_\alpha}{\partial t} + \frac{\partial \rho u_i Y_\alpha}{\partial x_i} = \frac{\partial \rho Y_\alpha V_{\alpha,i}}{\partial x_i} + \dot{\omega}_\alpha + \dot{m}\delta_{\alpha v} \tag{10}$$

$$\frac{\partial \rho h_s}{\partial t} + \frac{\partial \rho u_i h_s}{\partial x_i} = \frac{\partial}{\partial x_i}\left[\lambda \frac{\partial T}{\partial x_i} - \rho \sum_{\alpha=1}^{N} h_{s,\alpha} Y_\alpha V_{\alpha,i}\right] + \frac{dP}{dt} + \tau_{ij}\frac{\partial u_i}{\partial x_j} + \dot{\omega}_T + \dot{e} \quad (11)$$

the above system is complemented with the perfect gas equation of state

$$\rho = \frac{PW}{RT} \quad (12)$$

ρ, u_i, and T are the density, velocity component in the x_i-direction, and temperature of the mixture, respectively. P and p_1 are the thermodynamic and dynamic components of pressure. The quantity τ_{ij} is the viscous stress tensor, $V_{\alpha,i}$ is the i-component of the diffusion velocity of species α, $h_s = \sum_{\alpha=1}^{N_s} Y_\alpha h_{s,\alpha}$ represents the specific sensible enthalpy of the mixture and $h_{s,\alpha}$ is the sensible enthalpy of species α. The mass fraction of chemical species α is Y_α, $\delta_{\alpha v}$ denotes the Kronecker tensor, the value of which is unity if the species α matches the vapor index v, and zero otherwise. The quantities W_α and $W = (\sum_{\alpha=1}^{N_s} Y_\alpha / W_\alpha)^{-1}$ are the molecular weight of species α and the molecular weight of the reactive mixture, respectively. Finally, R is the universal gas constant.

Various source terms are present in the previous set of equations: $\dot{\omega}_\alpha$ and $\dot{\omega}_T$ are related to the chemical reaction processes whereas $\dot{m}$, $\dot{\mathbf{v}}$, and $\dot{e}$ result from the two-way coupling between the carrier phase and the spray. $\dot{\omega}_\alpha$ and $\dot{\omega}_T$ correspond to production/destruction rate of chemical species α and the resulting heat release rate, respectively. They are computed with the chemkin VODE solver using the n-heptane kinetics of Patel et al. [26], which contains 29 species and 52 elementary reactions. The terms $\dot{m}$, $\dot{\mathbf{v}}$, $\dot{e}$ are modifying the mass, momentum and temperature in the gaseous phase owing to a distribution of the

Lagrangian quantities on the Eulerian grid.

$$\dot{m}^{(n)} = \rho_d \frac{\pi}{4} \frac{1}{\mathcal{V}} \sum_k \alpha_k^{(n)} \frac{a_k^3}{\mathcal{T}_{a,k}} \tag{13}$$

$$\dot{\mathbf{v}}^{(n)} = -\rho_l \frac{\pi}{4} \frac{1}{\mathcal{V}} \sum_k \alpha_k^{(n)} a_k^3 \left(\frac{2}{3} \frac{\mathbf{u}(\mathbf{x}_k, t) - \mathbf{v}_k}{\mathcal{T}_{\mathrm{v},k}} - \frac{\mathbf{v}_k}{\mathcal{T}_{a,k}} \right) \tag{14}$$

$$\dot{e}^{(n)} = -C_l \rho_l \frac{\pi}{4} \frac{1}{\mathcal{V}} \sum_k \alpha_k^{(n)} a_k^3 \left(\frac{2}{3} \frac{T(\mathbf{x}_k, t) - T_k - B_{T,k} L_v / C_p}{\mathcal{T}_{T,k}} - \frac{T_k}{\mathcal{T}_{a,k}} \right) \tag{15}$$

where $\mathcal{V}$ is a control volume, $\sum_k$ is the sum performed over all droplets affecting the node n and $\alpha_k^{(n)}$ is the distribution coefficient of the k^{th} droplet source term on the node n. Considering all the nodes affected by droplet k, it is necessary to have $\sum_n \alpha_k^{(n)} = 1$ to conserve mass, momentum and energy during the Lagrangian/Eulerian coupling. The values of $\alpha_k^{(n)}$ are then the normalized distances between the droplet k and the surrounding nodes.

2.2. Configuration

As underlined in the introduction, all the simulations are carried out with a two-dimensional square domain although the evaporation process is kept three-dimensional. Similarly to [16], this would correspond to a thin slice of a 3D field with regularly spaced array of droplets in the third direction. A sketch of the computational domain is shown in figure 2. The side of the domain is 10 mm long. Both directions are periodic. They are discretized with an isotropic grid (256×256) keeping grid size $\Delta x = 39.2$ μm. The objective was to reduce as much as possible the computational cost since this configuration is considered as an extension of a chemical reactor that will need numerous executions to underline the impact of various spray physical parameters on gas autoignition.

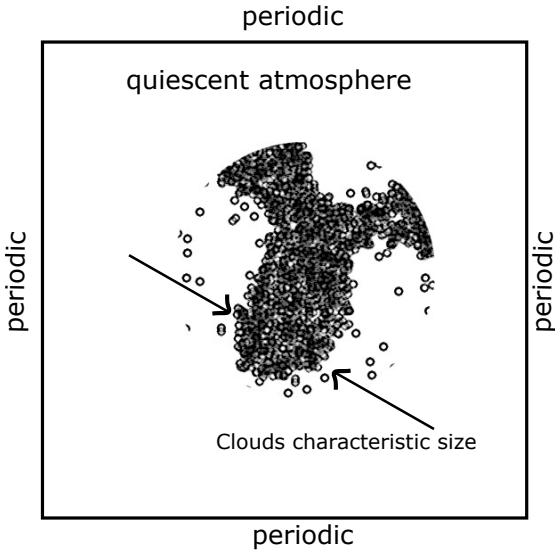

Figure 2: Sketch of the computational domain.

The generation of clouds of droplets with a prescribed characteristic size and density is based on a spectral procedure described by Reveillon [27]. It allows for generating turbulent velocity and scalar fields along with sprays, the variation of density of which is prescribed. Some details concerning the control of the preferential segregation are given here since it is the basis of the extended reactor configuration. First, it is necessary to define two probability density functions (PDF): the droplet diameter distribution into the spray $P(a)$ and the PDF $P(\xi)$ of the spray local density $\xi(\mathbf{x})$, which is the number of droplets per unit of volume. $P(a)$ may be characterized by any experimental or analytical shape (Log-Normal, Rosin-Rammler, ..., [28]) or by a delta function if a monodispersed spray is considered, which is the case in this paper. Thanks to the PDF of the spray density, which is prescribed via a β-function [29], it is possible to generate very different topology of clouds. The mean spray density $\overline{\xi}$ and $P(a)$ fix the global equivalence ratio of the configuration while the density variance $\overline{\xi^2}$, necessary to define the β-function, allows for controlling

the segregation level $S_L = \overline{\xi^2}/\overline{\xi}(1-\overline{\xi})$ of the clouds. If $S_L = 1$, a maximum segregation level is chosen but if $S_L = 0$ the droplets are uniformly and randomly distributed in the domain. A last parameter, δ_c is necessary to prescribe the characteristic size of the clouds. Examples of generated clouds are shown in figure 3. On the left, three figures (fig. 3-(a),(b),(c)) shows the same high level of segregation but the characteristic size of the clouds of droplets has been diminished from $\delta_c = 2.5\ mm$ (Fig. 3-(a)) down to $\delta_c = 0.83\ mm$ (Fig. 3-(c)). On the right, in figures 3-(a),(d),(e), the same characteristic cluster size is prescribed $\delta_c = 2.5\ mm$ but the segregation level varies from a highly segregated spray ($S_L \approx 1$) at the top (Fig. 3-(a)) down to a moderate segregation level spray ($S_L \approx 0.25$) at the bottom (Fig. 3-(e)). The whole generation procedure may be found in [27].

3. Reference Case: homogeneous spray autoignition

To identify the spray preferential segregation influence on autoignition, reactivity of a homogeneous mixture with similar thermodynamic conditions inside a zero-dimensional (0D) reactor has to be first characterized. Consequently, autoignition of a two-phase flow n-heptane/air mixture, necessarily homogeneous is used as reference. This configuration is very close to the reactor used by the authors in [16]. Therefore, no further detail is given here.

Figure 4 depicts two-phase flow n-heptane/air autoignition delay as a function of the gas initial temperature. The decrease of the autoignition delay with the increase of the initial gas temperature is reproduced everywhere except in the NTC domain. Even if only a skeletal chemical mechanism was used, the NTC domain is accurately represented, between 850 K and 1050 K in this study (Fig. 4). Inside this zone, the system reactivity falls down (autoignition delay becomes longer) while the initial temperature increases.

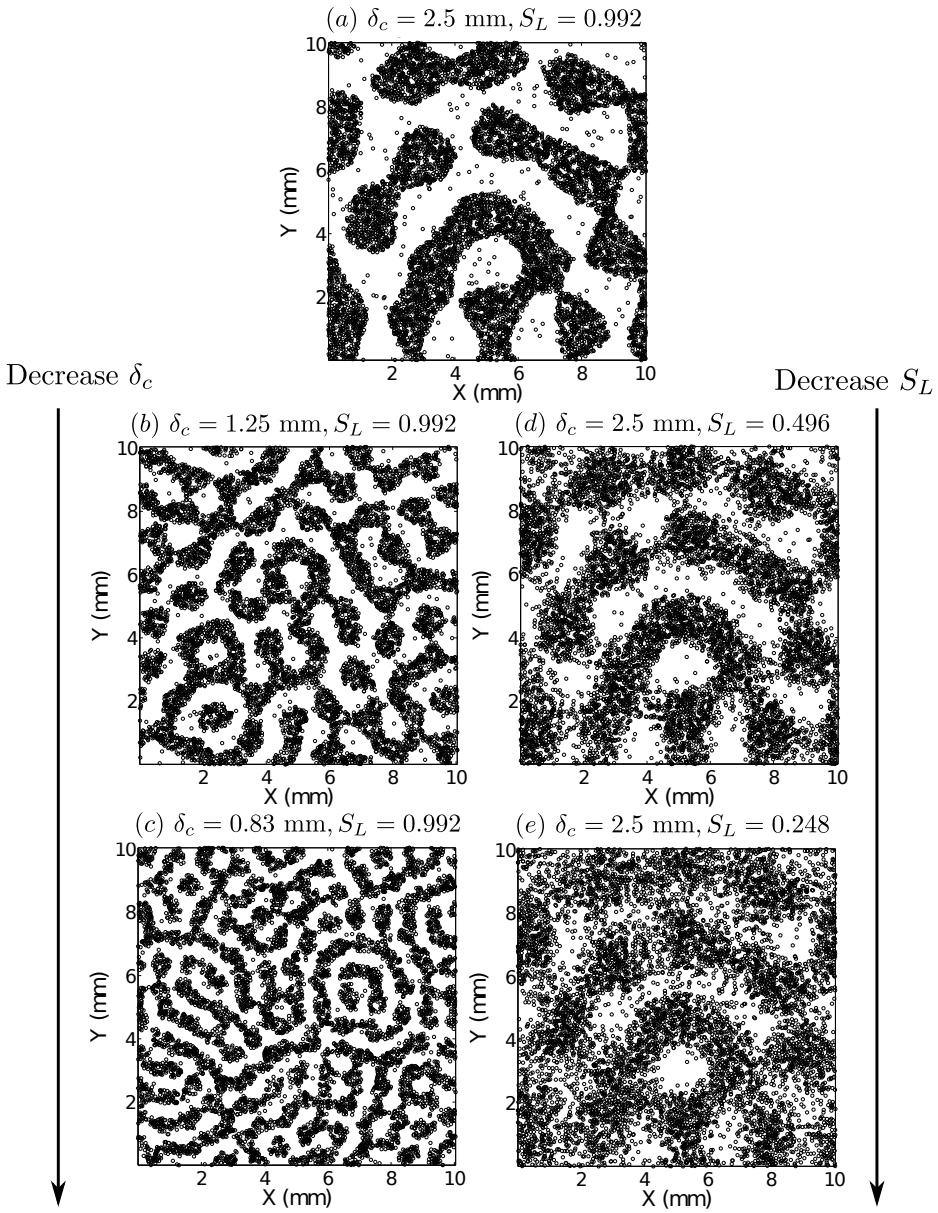

Figure 3: Initial repartition of the clusters of droplets with two prescribed parameters: the characteristic size of the clusters δ_c (left), and the segregation level S_L (right) through the control of the local droplet density.

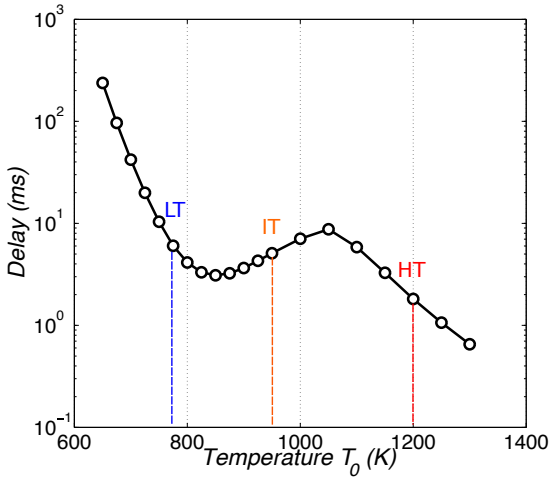

Figure 4: Autoignition delays of a stoichiometric and monodisperse two-phase flow n-heptane/air mixture for different initial temperatures. Initial droplet diameter and pressure are 2 μm and 10 bar, respectively.

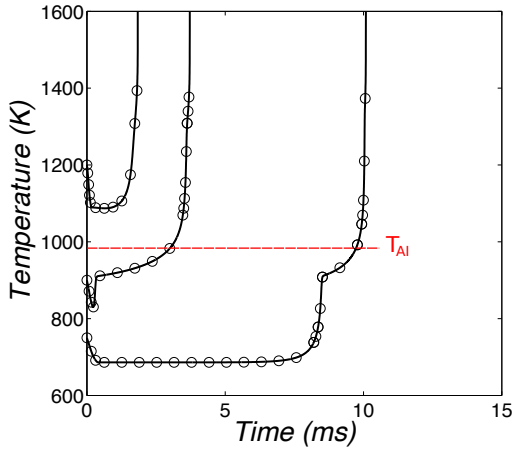

Figure 5: Temporal evolution of temperature for three initial gas temperature (T_0 = 1200, 900 and 750 K) in 0D (homogeneous) n-heptane/air two-phase flow reactor. Equivalence ratio is 1, initial droplet diameter and pressure are 10 μm and 10 bar, respectively

In purely gaseous case, the temperature range of the NTC domain is almost independent of the fuel/air equivalence ratio but shifts towards higher temperatures when pressure increases. On the contrary, in former study [16], authors have shown that in the case of spray autoignition the NTC region is

simultaneously influenced by the pressure and the equivalence ratio.

To analyze the impact of the initial gas temperature on the autoignition process, three distinct initial temperatures have been chosen with respect to the NTC temperature range to illustrate the various chemical processes that may be encountered in homogeneous reactors. First, a 'high' temperature level (`HT`, $T_0 = 1200$ K) has been considered, then an 'intermediate' (`IT`, $T_0 = 900$ K) and a 'low' (`LT`, $T_0 = 750$ K) temperature levels.

Figure 5 shows the temperature evolution versus time for the three homogeneous configurations. Whatever the considered case, the liquid vaporization presents a significant temperature decrease. This cooling effect is directly related to the amount of liquid mass receiving the heat flux. In addition of this initial temperature decrease, figure 5 also shows a direct impact of the initial temperature on the autoignition process. In contrast to hot temperature case which is characterized by a one-stage autoignition, the low and intermediate temperature cases present a two-stage autoignition. The first reaction stage increases the temperature of a few hundred degrees. This phase is called '*cool flame*'. It is a transition from low or intermediate temperatures to hot temperatures that provoke the second stage, which corresponds to the main autoignition. Note that the characteristics of *cool flames* depend both on the initial gas temperature and the gas-liquid heat transfers. Figure 5 also shows that the thermal runaway which characterizes the main autoignition, takes place from a fixed temperature threshold whatever the initial temperature.

4. Autoignition location

4.1. Effect of initial gas temperature

To analyze the impact of the initial gas temperature on autoignition in a heterogeneous system (Fig. 3-(a)), a single spray distribution (monodisperse spray)

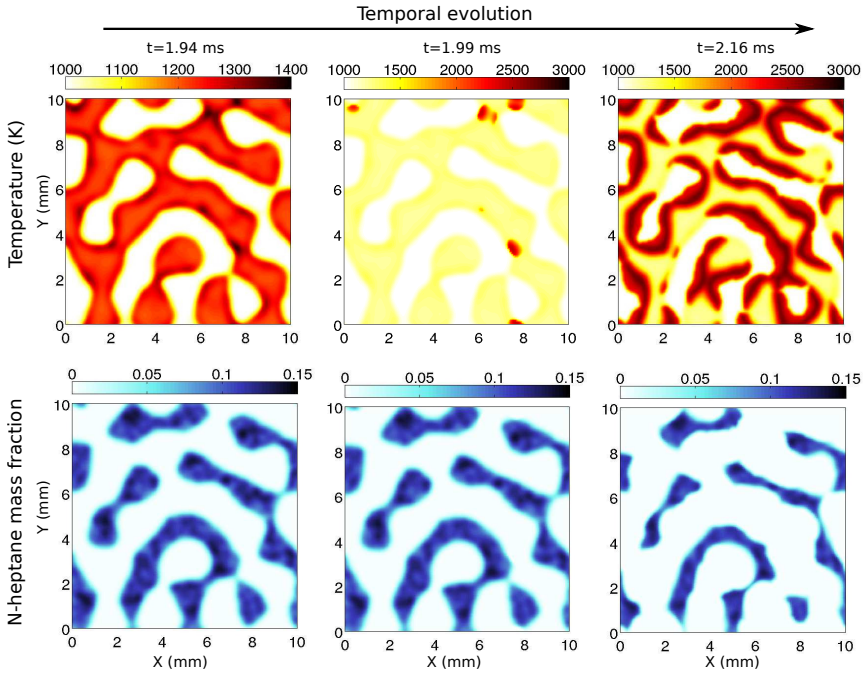

Figure 6: Autoignition of a n-heptane/air mixture with a highly segregated spray (Fig. 3-(a)). Homogeneous initial air temperature: $T_0 = 1200$ K. Top: temperature evolution (K); bottom: n-heptane vapor mass fraction evolution

has been used with an initial droplet diameter $a_0 = 10\ \mu m$ ($a_0/\Delta x < 0.3$) and a global equivalence ratio equal to 1. The non-monotonous evolution (NTC region) of the autoignition delay as a function of the temperature and the apparition of *cool flames* for some other specific temperature ranges make analyses more difficult. It is then necessary to vary initial temperature to understand physical phenomena present in the two-phase flows autoignition. This study is based on the same temperature levels introduced in the reference case (HT,IT,LT).

4.1.1. High temperature (HT)

To vaporize, n-heptane droplets capture an important amount of energy available in the hot gases. Heat exchanges between gas and liquid phases induce

localized decreases of the gas temperature that may be seen in Fig. 6-(Top) at $t = 1.94$ ms, for example. These 'colder' zones are directly related to the pocket of vapor of fuel that have been formed (Fig. 6-(bottom)). At time $t = 1.99$ ms, autoignition spots appear in the computational domain (Fig. 6-(middle), see red spots). They are mostly localized in the preheated areas at the edges of the pockets of fuel vapor in direct contact with the hot zone.

In an initially quiescent environment, the existence of high temperature gradients due to droplet vaporization induces a weak advection process that is directly linked to the density difference between hot and cold zones. Along with the molecular diffusion, advection promotes secondary autoignition areas (Fig. 6-(top), time $t = 2.16$ ms) and leads to a succession of ignition processes. Fig. 6 shows how, in this specific temperature case, the reactive process starts from the external frontiers of the vapor pockets and propagates inside. This process is scrutinized in figure 7-(a) where the gas temperature (top) and the vapor mass fraction (bottom) evolutions have been plotted. Profiles are based on the most reactive pocket (Fig. 6, $X = 7.5$ mm and 4.5 mm $< Y <$ 10 mm).

At time $t = 0.77$ ms, prior to any significant heat release, two areas that are fuel rich (stoichiometry $Y_v^{st} = 0.0625$) are clearly visible in figure 7-(a)-bottom with a vapor mass fraction approximately equals to 0.13. These peaks are directly linked to a 'low' temperature level ($T \approx 970\ K$), compared to the initial gas temperature ($T_0 = 1200\ K$), Fig 7-(a)-bottom. As previously stated, it is the direct consequence of the heat transfer during the droplet vaporization process. This high temperature gap is far from being negligible, especially from the autoignition point of view, which is highly non-linear. Note that even if the local mixture is rich, stoichiometry in the whole reactor is respected from an average point of view. This kind of non-homogeneous configuration can be encountered in practical cases since preferential segregation due to the turbulent

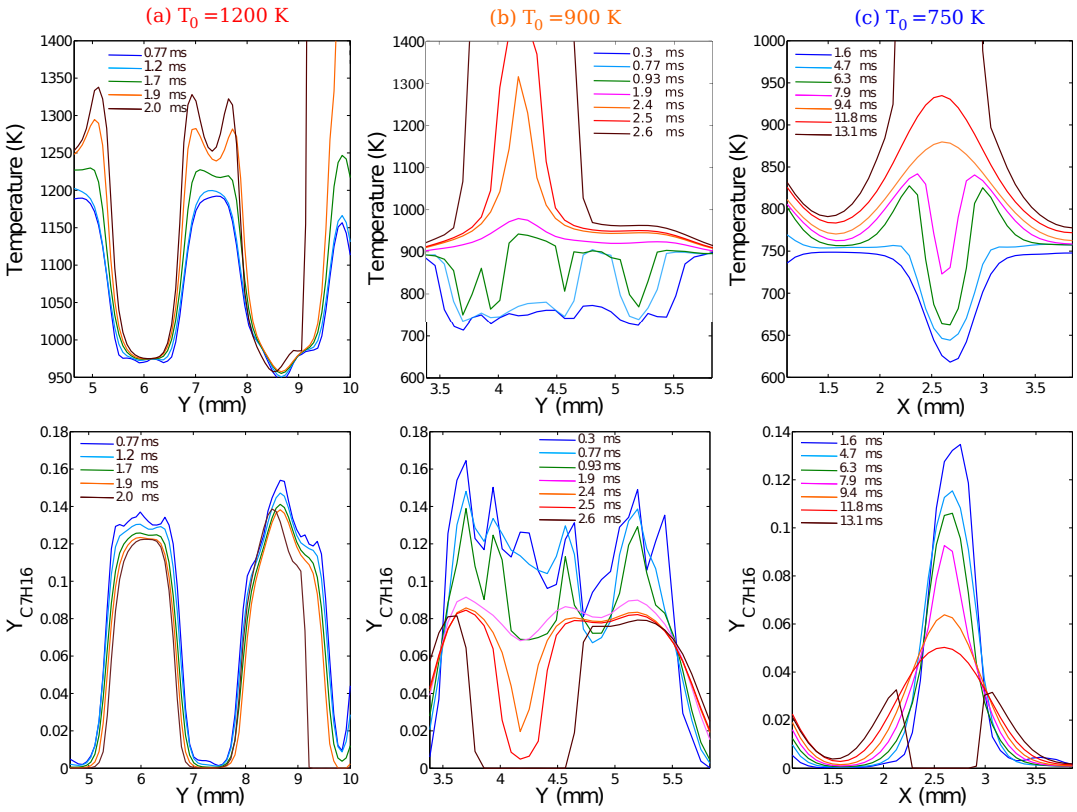

Figure 7: Temporal evolution of the gas temperature (top) and the fuel-vapor mass fraction (bottom) profiles at the most reactive level for three different initial gas temperatures T_0 = 1200, 900 and 750 K (left to right).

flow may lead to a strongly non-homogeneous droplet dispersion [30].

Starting at time $t = 1.2$ ms, a temperature increase may be observed at the periphery of the vapor pockets, mostly on the hot gas regions in the lean side of the vapor mass fraction, see the double temperature peak forming at positions $Y = 6.8$ mm and $Y = 7.8$ mm in (Fig. 7-(a)). Significant heat release represented by peaks of temperature is clearly visible at time $t = 2$ ms and at position $Y = 6.8$ and 7.7 mm, among others. This indicates that the autoignition is controlled by the mixing (diffusion) zones in this quiescent configuration.

4.1.2. Intermediate temperature (IT)

In the intermediary temperature case ($T_0 = 900$ K), the autoignition process presents completely different evolution from the previous high temperature ($T_0 = 1200$ K) configuration. This difference is linked to the chemical mechanism that characterizes this temperature range. Figure 8-(top) shows snapshots of the temperature obtained at three instants of the autoignition process. The corresponding vapor fields are shown in figure 8-(bottom).

Time $t = 0.3$ ms shows first the cooling effect of the vaporization on both the temperature and the vapor fields prior to any significant chemical reaction. Then, at time $t = 1.88$ ms, we observe a general increase of the temperature in all the areas initially occupied by droplets. The temperature increase remains moderated, compared to a full ignition, and it leads to a partial consumption of the fuel vapor. The corresponding vapor and the temperature profiles have been plotted in figure 7-(b). Profiles are extracted from a cut through a single pocket of fuel that corresponds to the most reactive area of the flow (Fig. 8-right ($t = 2.66$ ms), $X = 1.6$ mm and 3.4 mm $< Y <$ 5.8 mm).

As shown in figure 7-(b), after evaporation, a moderate temperature increase of 150 K is observed inside the fuel rich pockets of vapor at time $t = 0.77$ ms, quickly followed by an elevation of temperature in the domain starting at time

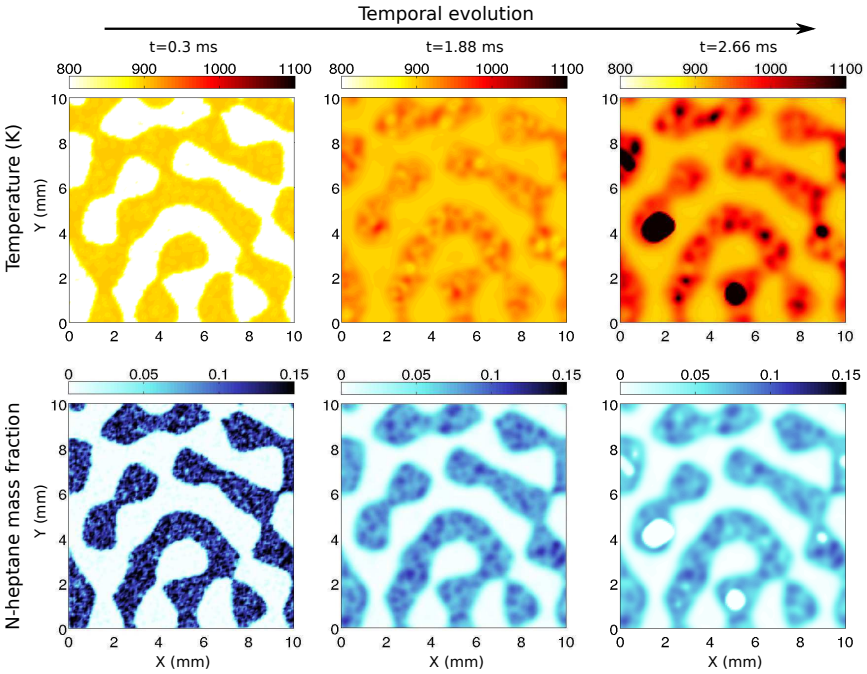

Figure 8: Autoignition of a n-heptane/air mixture with a highly segregated spray (Fig. 3-(a)). Homogeneous initial air temperature: $T_0 = 900$ K. Top: temperature evolution (K); bottom: n-heptane vapor mass fraction evolution

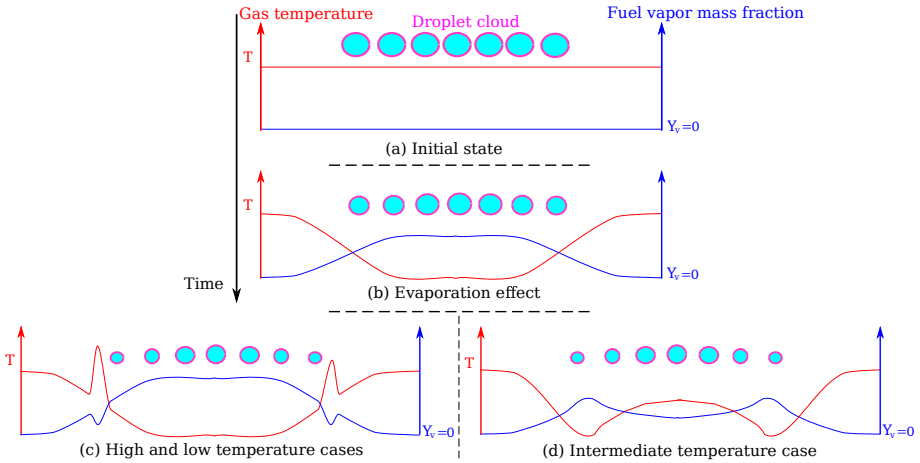

Figure 9: Localization of the most reactive zone: sketch of the evolution of gas temperature and vapor mass fraction profiles through area initially occupied by droplets.

$t = 0.93$ ms. It leads, at time $t = 1.9$ ms to an almost uniform temperature inside and outside the pocket of fuel vapor. In fact, a *cool flame* has appeared in the pocket of fuel and the heat release due to the *cool flame* has compensated the heat loss due to vaporization.

This first autoignition phase is then followed at time $t = 1.9$ ms by the complete autoignition of the mixture of the considered area (Fig. 8-(bottom), $t = 2.66$ ms). The autoignition process occurs in the core of the droplet cluster in a slightly rich area and then it propagates toward the edges. The fact that the initial temperature is within the NTC range (where the reactivity is inverted with respect to the temperature increase), autoignition is then promoted not only by the temperature decreases due to the vaporization, but also by the amount of fuel vapor available to autoignite (rich mixture). On the other hand, the main ignition process lead to a total consumption of the vapor of fuel and 'holes' may be observed in figure 8-(bottom), time $t = 2.66$ ms, for example.

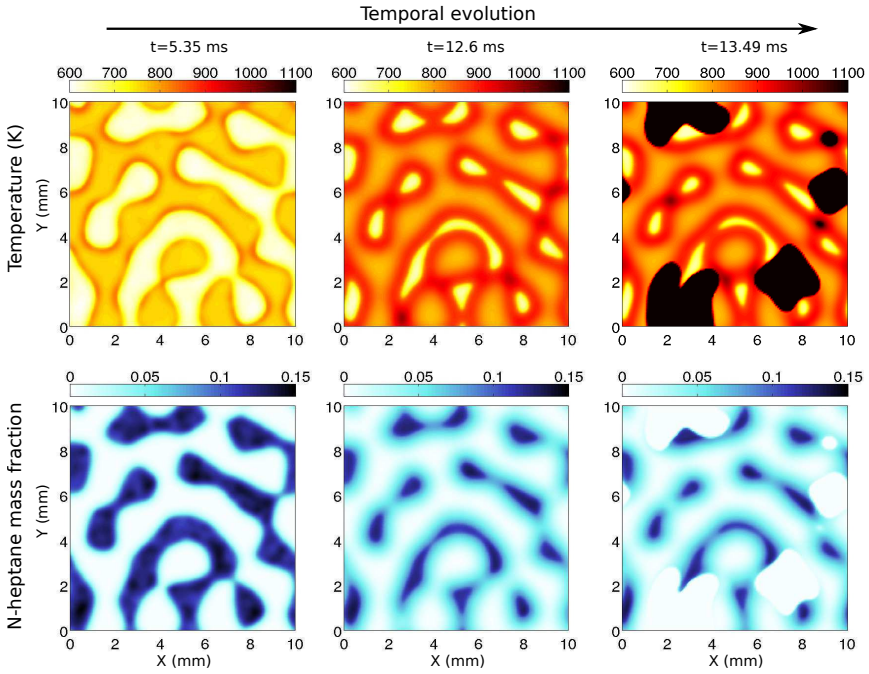

Figure 10: Autoignition of a n-heptane/air mixture with a highly segregated spray (Fig. 3-(a)). Homogeneous initial air temperature: $T_0 = 750$ K. Top: temperature evolution (K); bottom: n-heptane vapor mass fraction evolution

4.1.3. Low temperature (LT)

In the 'low' temperature case ($T_0 = 750$ K), autoignition of the highly segregated spray follows a third scenario compared to the former cases. Figure 10 shows snapshots of temperature and vapor fields at three times. Very quickly at $t = 5.35$ ms, it is possible to observe the apparition of *cool flames* at the edges of the areas initially occupied by the droplets (Fig. 10-top-left). Consequently the temperature reaches 850 K around all the fuel vapor pockets. Then this phenomenon propagates toward the center of the pockets by burning partially the available vapor of fuel (Fig. 10-center). Then, the main autoignition occurs at the bridges between close pockets. These bridges are defined by the shorter distance separating two pockets of fuel. In this area, the *cool flames* standing at the boundaries fill more rapidly the pocket inter-distance. Therefore, the heat losses toward cold areas undergone by the *cool flames* is strongly limited since there is less contact with cold zones. Then, the high energy of these 'bridges *cool flames*' promotes the main autoignition. These observations are confirmed by the evolution of the temperature and the vapor profiles. The most reactive area has been selected and analyzed in figure 7-(c) at the position $Y = 0.5$ mm and 1 mm $< X <$ 4 mm. Between times $t = 1.6$ ms and $t = 7.9$ ms (Fig. 7-(c)), the *cool flames* apparition at the edge of the cluster are clearly visible ($X = 2.25$ mm and $X = 3$ mm) through a double temperature peak. Later, at time $t = 9.4$ ms the 'bridge *cool flame*', resulting from the union of two initially separated flame, is formed. Then, the energy being high enough, the main autoignition occurs.

Figure 9 displays the evolution of the gas temperature and the mass fraction profiles from the initial state to the beginning of autoignition. Figure 9-(a) represents the initial state of monodisperse spray with an uniform initial gas composition and temperature, and the figure 9-(b) represents the effect of the

vaporization on the temperature and the mass fraction profiles whatever the initial temperature of the gas. We can notice that the strong preferential segregation of the droplets generates stratified zones in which the temperature decreases with the amount of fuel vapor. In our case (quiescent flow), these areas are mainly controlled by thermal and molecular diffusion. Since, there are two scenarios concerning the localization of the most reactive zones, it depends on the initial temperature of the gas mixture. The first scenario shown in figure 9-(c) is representative of autoignition of mixtures initially at low and high temperature, in such cases *cool* flames and *main flames* occur at the edges of droplet clusters and propagate towards the center. It should be noticed that, unlike hot temperature cases, our simulation shown that the main autoignition in low temperature case occurs within droplet cloud. The second scenario shown in figure 9-(d) provides an overview of the autoignition of the mixtures initially at intermediate temperature (NTC region). In this case the *cool flame* and the main autoignition are favored by the local cooling associated with a high equivalence ratio, therefore, both steps take place inside the cluster.

Furthermore, we have observed that the presence of *cool flames* gives rise to autoignition within cloud of droplets. This can be explained by the existence of the autoignition triggering temperature previously discussed in reference homogeneous case (Fig. 5). Indeed, *cool flames* increase the local temperature of the mixture to the temperature T_{AI}, so that the temperature level become almost uniform in the cluster. This process promotes the autoignition inside the center far from the edges where the thermal and molecular diffusions brake the thermal runaway.

4.2. Impact of the size of the clusters

As detailed previously, the liquid phase topology in the segregated reactor is characterized by two main parameters: the characteristic size of the clusters

δ_c and the droplet segregation level S_L. In practical configurations, these properties are mainly controlled by the atomization process and droplets-turbulence interactions. To begin with, our objective is to study the influence of these parameters on the autoignition but first independently of any turbulent flow (turbulent flow will be considered in the next section). That is why we continue here with non-homogeneous reactor containing a quiescent atmosphere. Three clusters characteristic sizes and three segregation levels have been prescribed. Any configuration may be studied thanks to the method described in [27]. Five configurations (parameters: δ_c and S_L) have been selected, they are visible in figure 3. All other parameters and properties are identical: high temperature environment ($T_0 = 1200$ K, pressure $P_0 = 10$ bar), stoichiometric global equivalence ratio and an initially monodispersed spray, the diameter of the droplets being $a_0 = 10$ μm.

Let's remember that there is no *cool flame* in 'high' temperature cases. Indeed, the amount of energy is high enough to lead to a quick and complete autoignition without any major influence of the transport phenomena. Thus, the initial temperature $T_0 = 1200$ K has been selected in this analysis in order to observe if there is a direct impact of the spray topology on the main autoignition delay. Figure 11 presents the ignition spots of all configurations. From a purely topological point of view, all ignition spots follow a similar behavior and they appear mostly at the periphery of the clusters whatever their characteristic size.

Figure 12-left shows the impact of the variation of the cluster characteristic size on the evolution of the mean temperature (average over the domain) and its deviation. First, the decrease of the cluster size increases the system reactivity leading to an early autoignition. Second, the temperature fluctuations decreases by diminishing the cluster characteristic size. Both observations are the direct

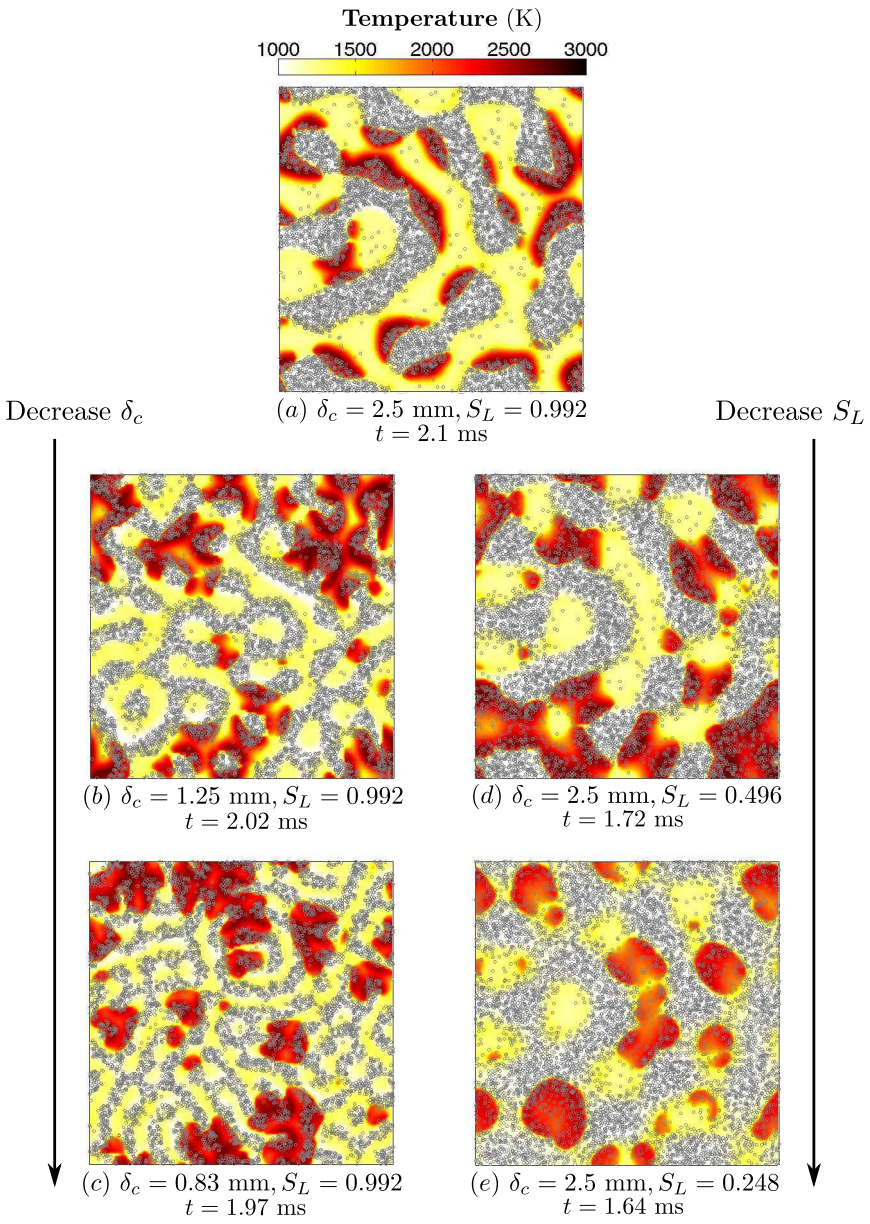

Figure 11: Autoignition of segregated sprays. 'High' temperature case ($T_0 = 1200\ K$). Left: variation of the characteristic size of the clusters; right, variation of the segregation level.

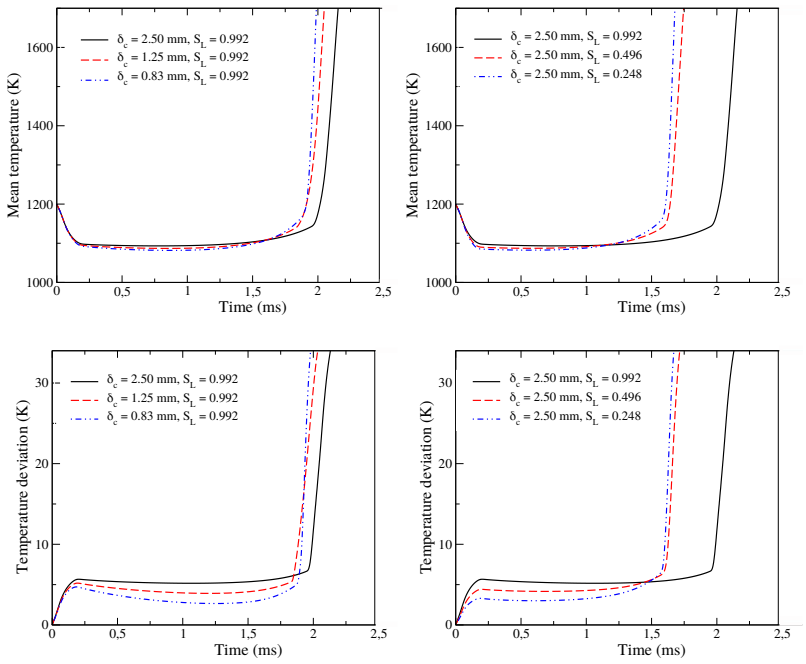

Figure 12: Influence of clusters characteristic size variation (left) and segregation level variation (right) on the mean temperature and the temperature deviation of cases in figure 11.

consequence of the increase of the exchange surface between clusters and the hot air, which increases the number of points with the most reactive region. The increase exchange surface also produces more thermal and mass diffusion, and, accordingly a reduction of the local temperature and equivalence ratio fluctuations.

The decrease in the segregation level (Fig. 12-right) causes the same effects concerning the temperature deviation temperature and the system reactivity. This tendency remains valid at 'high' and 'low' temperatures. Conversely, if the initial temperature of liquid belongs to the 'intermediate' temperature range, the reactivity can be promoted by a strong local equivalence ratio. In this case, the decrease of the segregation level may delay the autoignition process.

5. Autoignition in turbulent flows

The objective of this section is to add the impact of the turbulent gas fluctuations on the most reactive areas and to observe whether there are correlations between the most reactive regions, the scalar dissipation levels and the vorticity intensity. Two-dimensional simulations are performed in a square domain of 10 mm by 10 mm. Segregated liquid droplets are embedded in a decreasing homogeneous isotropic turbulence. The turbulent gas velocity field is initialized by specifying a Passot-Pouquet isotropic energy spectrum [27]. The initial velocity root mean square u_{rms} is 1.2 m/s, the integral length scale is 0.75 mm and the Kolmogorov length scale is 55.4 μm. The initial droplet velocity was set to zero to isolate the effect of the carrier phase based on the comparison with the previous cases. A 256×256 isotropic Cartesian grid is used ($\Delta x = 39.2$ μm) to capture all the scales of the turbulent flow. Like in the quiescent case, the different initial gas temperatures HT, IT, LT were used: $1200, 900$, and 750 K, respectively. The initial pressure for all cases is 10 bar and the global equiva-

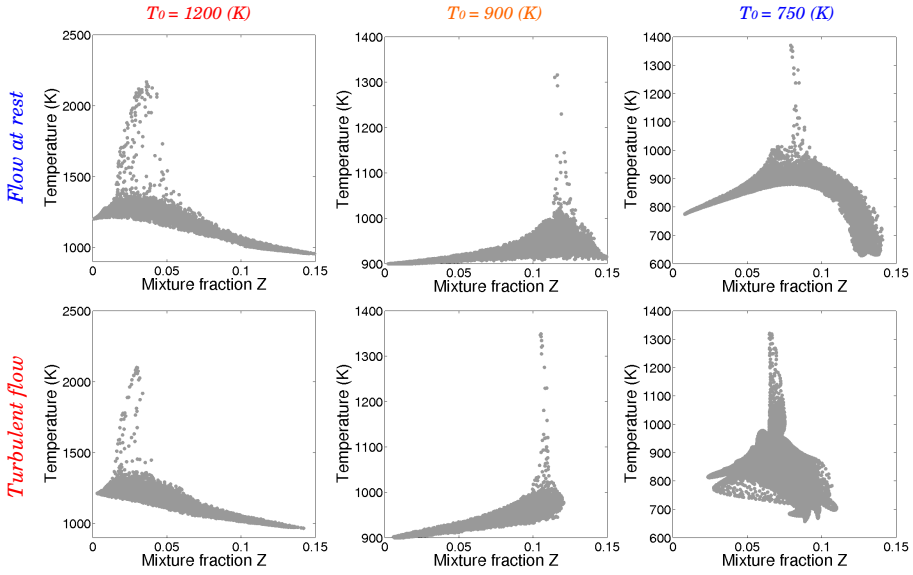

Figure 13: Scatter plots of carrier-gas temperature against mixture fraction for three initial gas temperatures ($T_0 = 1200,\ 900$ and 750 K) and for two scenarios: (I) flow at the rest (top) and (II) turbulent flow (bottom).

lence ratio is 1. The liquid properties are also similar to the previous quiescent study (initial droplets' diameter and temperature are 10 μm and 300 K, respectively).

5.1. Most reactive mixture fraction

Mixture fraction Z characterizes the mixing between all fundamental elements of a heterogeneous mixture [31]. Z is equal to 1 in a pure fuel stream and to 0 in the oxidizer stream. As far as complex chemistry is concerned, various definitions are possible [32, 33] for the mixture fraction. In this work, the mixture fraction Z of the flow is based on the vapor of fuel mass fraction. Indeed, one focuses on the combustion of n-heptane and the definition from [34] has been selected.

In the framework of two-phase flows, it is possible to demonstrate [35] that Z is not anymore an inert scalar since its time evolution implies the apparition of

a mass source term due to droplet vaporization. It is important to characterize Z accurately since it is the key parameter of any combustion model. Therefore, an analysis of the ignition process in the mixture fraction phase space may offer a lot of information for model developments and their applications.

One of the key parameter, when studying autoignition, is to determine the value of Z corresponding to the area where the first autoignition spots are detected. It is called the 'most reactive' mixture fraction Z_{MR}.

Figure 13 presents scatter plots of the gas temperature against the mixture fraction for two different scenarios: (I) flow at rest (Fig. 13- top) and (II) turbulent flow (Fig. 13- bottom). Both have been applied with the three reference temperature levels ($1200, 900$, and 750 K). The scatter plots reveal that: (1) ignition occurs first at certain values of mixture fraction (Z_{MR}), the value of which depends on the initial gas temperature. (2) A comparison between the Z_{MR} values with initial turbulence flow and those with flow at rest indicates that the turbulent flow has a weak influence on the most reactive mixture fraction at this turbulence level. Note that even if the initial velocity root mean square is the same for all three cases (HT, IT and LT) it reaches different levels at autoignition time since turbulence is decaying and the autoignition delay is different for each case.

Indeed, in the 'high' temperature case ($T_0 = 1200$ K) and for both scenarios, figure 13-left shows that the first significant heat release spots are characterized by a most reactive mixture fraction of around 0.025, which corresponds to a gaseous equivalence ratio equals to 0.39. This tendency to ignite in a lean environment is confirmed by the work of Wang and Rutland [8] who observed a similar Z_{MR}, although, quantitative comparisons are not possible since pressure and temperature conditions were different (1 bar, 1700 K, respectively). The gap between the one-phase and two-phase Z_{MR} is directly linked to the presence

of the liquid phase that delays autoignition of the rich mixture because of the proportionally strong decrease of the local temperature. It has been shown by Bouali et al. [16] and Wang and Rutland [8].

For 'intermediate' temperature, ($T_0 = 900$ K, Fig. 13- center), the evolution of temperature as a function of the mixture fraction is different. The first main heat release spots are localized in rich areas ($Z_{MR} = 0.115$). This Z_{MR} corresponds to a main ignition. It follows a *cool flame* creation which is localized in a Z_{MR} area that is less rich (around the stoichiometry).

As far as 'low' temperature ($T_0 = 750$ K) is concerned, the most reactive mixture fraction corresponding to the *cool flame* autoignition is very small. It explains why the *cool flames* are mostly located at the edge of the fuel pockets. Indeed, it needs only a small amount of fuel to ignite since it is favored by relatively high local temperature levels. On the contrary, the main autoignition spots are situated in slightly rich areas (Fig. 13- right) where $Z_{MR} = 0.08$ (to be compared with the stoichiometric value: $Z^{st} = 0.0625$), *i.e.*, where the fuel vapor quantity is sufficient to start-up the main autoignition.

Figure 14 shows instantaneous snapshots of early autoignition of temperature, mixture fraction, vorticity and scalar dissipation:

$$\chi = \left(\frac{\partial Z}{\partial x}\right)^2 + \left(\frac{\partial Z}{\partial y}\right)^2 \quad , \tag{16}$$

at time $t = 1.88$ ms, $t = 2.59$ ms and $t = 7.08$ ms for the reference temperatures, HT, IT, LT, respectively; the first autoignition sites embedded in the temperature fields (black spots) are shown in the other fields by iso-contours (red color). The first autoignition spots are located in areas of low scalar dissipation rate, where mixture fraction gradients are relatively small and where there is an adequate mixing level. These zones appear also if the turbulence

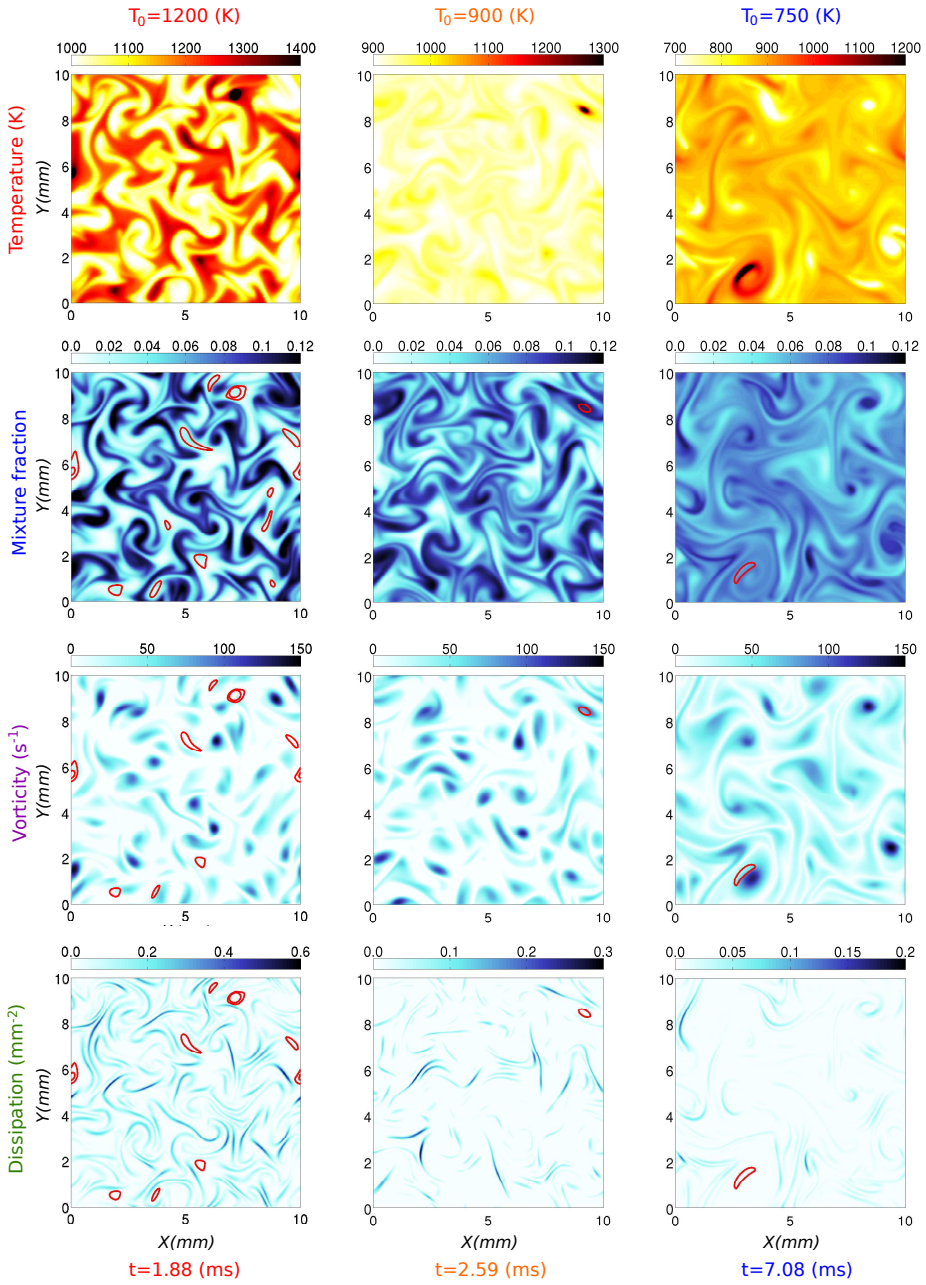

Figure 14: Snapshots of temperature (K), mixture fraction, vorticity (s^{-1}) and scalar dissipation (mm^{-2}) (top to bottom) for three initial gas temperatures $T_0 = 1200$, 900 and 750 K (left to right) at the moment of the ignition. Red iso-contours indicate the most reactive regions.

intensity and the mean value of strain rate are high. This result fully matches the outcomes in [9, 1, 36, 3], where a simpler chemistry models for n-heptane was used, and in [7, 8] where a skeletal chemical mechanism for same fuel was considered. Studies [37, 38] using a reduced chemical mechanism for hydrogen confirm this remark. This observation is valid whatever the initial gas temperature. This finding proves the importance of fluid dynamic phenomena in the autoignition process.

Unlike scalar dissipation rate, the existence of a correlation between vorticity magnitude and the first autoignition areas is not verified as figure 14 shows that the first autoignition spot may occur at low (HT case), medium (IT case) and strong (LT case) vorticity magnitude.

5.2. Average temperature over the Extended Reactor

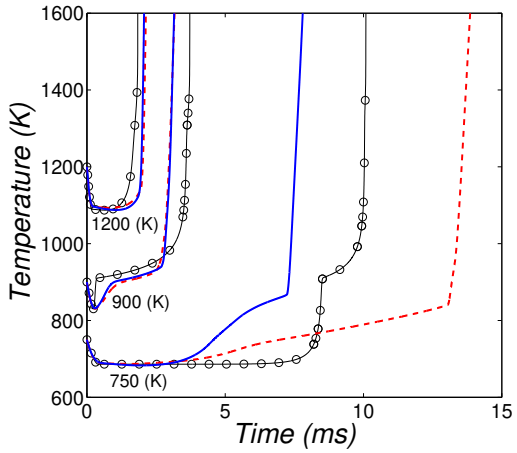

Figure 15: Average over the spatial domain of the gas temperature for spray autoignition configurations. Three initial gas temperature are compared ($T_0 = 750\ K$, $900\ K$ and $1200\ K$) for three initial scenarios: (I) segregated reactor with flow at rest, red dashed lines ; (II) segregated with turbulent flow, blue solid line; (III) homogeneous droplet distribution (0D reactor), circles with black solid line.

The influence of the initial gas temperature on the location of the first autoignition spots in a segregated two-phase flow has been studied in the previous

part. To complete this study, it is interesting to analyze the impact of segregated spray on the mean temperature in the reactor. Our objective is to extend classical autoignition studies of homogeneous mixtures or two-phase flows in 0D reactors to non-homogeneous configuration with droplet dispersion. Therefore the averaged output of our multidimensional reactor has to be compared to a 0D two-phase flow autoignition reactor. The input of both reactors are the same except for the segregation of the droplets. Note that it has been checked that our multidimensional reactor used with a uniformly distributed spray gives exactly the same result than a usual 0D reactor. Details concerning autoignition of homogeneously distributed two-phase flows may be found in [16].

The volume-averaged gas temperature of three scenarios is shown in figure 15. The initial temperatures ($T_0 = 750$ K, 900 K and 1200 K) and stoichiometric global mean equivalence ratio of the three scenarios that have been compared are similar. The only difference lays in the high segregation level of the segregated reactors and the nature of the flow: scenarios (I) and (II) correspond to a segregated reactor, (I) with flow at rest and (II) with turbulent flow; scenario (III) is the homogeneous reactor (0D).

The 'low' temperature case with segregated scenarios (I) and (II) generates a first exothermic chain of reactions that occurs earlier ($t = 5$ ms) than in scenario (III) ($t = 8$ ms), the homogeneous reactor. It corresponds to the apparition of the *cool flame* at the edges of the pocket of fuel. In segregated droplets, ignition occurs at an earlier stage since (1) in areas where droplets are present, the mass of vapor increases more rapidly and (2) outside these areas, the temperature remains at its initial level whereas it decrease everywhere in the homogeneous scenario (III). Therefore thermochemical conditions to initiate a reaction (a *cool flame*, given the temperature range) appear more quickly in the segregated scenarios.

Once the *cool flame* occurs in the homogeneous scenario, the mean temperature reaches very quickly 900 K. It induces very quickly the main autoignition process ($t = 10$ ms). On the other hand, temperature elevation in the segregated scenarios is generally slower because the temperature field resulting from the vaporization is also segregated and its evolution depends not only on localized reactive processes but also on diffusion and advection phenomena, the characteristic times of which are larger. Note that for scenario (II), even if the elevation of global *cool flame* temperature is relatively slow, it is much quicker than scenario (I). This is due to the turbulent flow that promotes the autoignition propagation.

For 'low' initial carrier-gas temperature, the figure 15 shows that the mixture heterogeneity may decrease or increase the reactivity of the system depending on the scenario. Indeed, the main autoignition is governed by segregation and transport phenomena. If the *cool flame* delay resulted from the homogeneity is greater than the elevation temperature delay caused by the heterogeneity, the segregation increases the system reactivity (scenario (II)). Otherwise, the system reactivity decreases (scenario (I)).

In the 'intermediate' temperature range ($T_0 = 900$ K), the general behavior of autoignition is the same but its characteristics change: (1) we see quick decrease of the mean temperature to vaporize the liquid phase. The same delay is necessary (less than 1 ms) in the three scenarios. (2) Then a *cool flame* appears in all reactors. It leads to a quick increase of the mean temperature in the homogeneous case while it is more gradual in the segregated ones. (3) Finally, autoignition occurs with delays that are slightly different. Indeed, ignition of segregated scenarios occurs half a millisecond earlier (2.5 ms versus 3 ms). It is directly linked to the topology of the flow, because, in this case, ignition occurs in the core of the pockets of fuel whereas in the two other cases (low an

high temperature), it is localized at the edges and much more dependent on temperature/vapor diffusion.

At high temperatures ($T_0 = 1200$ K), the heterogeneity of the mixture delays slightly the autoignition, despite the fact that the segregation creates favorable autoignition sites. These areas have suffered of reduced heat losses and their mixture fractions are equal to the most reactive mixture fraction for $T_0 = 1200$ K ($Z_{MR} = 0.025$). However, these sites are regions where strong heat and mass exchanges exist, thus they are characterized by high scalar dissipation rates that delays ignition. In practice, the first autoignition site located in the most reactive region in the segregated case appears at time $t = 1.88$ ms, while the autoignition in a homogeneous reactor (no scalar dissipation region) of a stoichiometric mixture occurs at time $t = 1.84$ ms.

As a first conclusion, it is first possible to state that the presence of a segregated spray delays autoignition, but only with some specific conditions, an earlier start is possible. Second, the spray segregation does not suppress the *cool flame* process. On the contrary, various topologies of *cool flames* have been observed and they strongly impact the flow evolution.

6. Conclusion

This study extend the chemical reactor configuration to investigate the effect of preferential segregation on autoignition of n-heptane/air two-phase flow. An Eulerian description is employed to solve the carrier-gas phase and a Lagrangian approach is used to track the liquid-fuel droplet properties. Two-way coupling interaction is considered through the exchange of mass, momentum, and energy between the carrier-gas phase and the dispersed phase. To describe the chemical reaction paths, a chemistry mechanism with 29 species and 52 reactions was

chosen. The effects of initial gas temperature (750, 900 and 1200 K) and droplet segregation were examined. The main findings are:

1. The presence of a segregated spray mainly delays of the autoignition, but only under some specific conditions, an earlier start is possible.
2. The spray segregation does not suppress the *cool flame* process. On the contrary, various topologies of *cool flames* have been observed and they strongly impact the flow evolution.
3. Important impacts of initial carrier-gas temperatures on the localization of the first autoignition sites has been identified. This is the consequence of non-monotonic dependence of Z_{MR} on initial gas temperature.
4. In agreement with previous literature, this study shows that first autoignition spots always occur at locations with lower scalar dissipation. The strong scalar dissipation can even control the ignition more than Z_{MR} parameter.
5. For the level of turbulence intensity chosen for this study, the values of Z_{MR} are weakly influenced by the turbulent flow and no correlation has been established between the first autoignition site and the vorticity magnitude. Indeed, the autoignition may occur at low as well as high vorticity magnitude.

7. Acknowledgments

The authors acknowledge the financial support from IFPEN. A part of this work has been performed using high-performance computing (HPC) resources from GENCI (Grand Equipement National de Calcul Intensif)-[CINES/IDRIS] under Grant A0052B07456.

References

[1] E. Mastorakos, T. A. Baritaud, T. J. Poinsot, Numerical simulations of autoignition in turbulent mixing flows, Combustion and Flame 109 (1-2) (1997) 198–223.

[2] S. Sreedhara, K. Lakshmisha, Autoignition in a non-premixed medium: Dns studies on the effects of three-dimensional turbulence, Proceedings of the Combustion Institute 29 (2) (2002) 2051–2059.

[3] A. Viggiano, V. Magi, A 2-d investigation of n-heptane autoignition by means of direct numerical simulation, Combust. Flame 137 (2004) 432–443.

[4] A. Viggiano, Exploring the effect of fluid dynamics and kinetic mechanisms on n-heptane autoignition in transient jets, Combustion and Flame 157 (2010) 328–340.

[5] R. Sankaran, H. G. Im, E. R. Hawkes, J. H. Chen, The effects of non-uniform temperature distribution on the ignition of a lean homogeneous hydrogene/air mixture, Proceedings of the Combustion Institute 30 (1) (2005) 875 – 882.

[6] E. Mastorakos, Ignition of turbulent non-premixed flames, Prog. Energy Combust. Sci. 35 (2009) 57–97.

[7] Y. Wang, C. Rutland, Effects of temperature and equivalence ratio on the ignition of n-heptane fuel spray in turbulent flow, Proc. Combust. Inst. 30 (2005) 893–900.

[8] Y. Wang, C. Rutland, Direct numerical simulation of ignition in turbulent n-heptane liquid-fuel spray jets, Combustion and Flame 149 (2007) 353–365.

[9] P. Schroll, A. Wandel, R. Cant, E. Mastorakos, Direct numerical simulations of autoignition in turbulent two-phase flows, Proceedings of the Combustion Institute 32 (2) (2009) 2275 – 2282.

[10] E. M. G. Borghesi, R. S. Cant, Complex chemistry dns of n-heptane spray autoignition at high pressure and intermediate temperature conditions, Combustion and Flame 160 (2013) 1254–1275.

[11] A. Abdelsamie, D. Thévenin, Direct numerical simulation of spray evaporation and autoignition in a temporally-evolving jet, Proceedings of the Combustion Institute 36 (2017) 2493–2502.

[12] A. Neophytou, E. Mastorakos, R. Cant, Complex chemistry simulations of spark ignition in turbulent sprays, Proceedings of the Combustion Institute 33 (2) (2011) 2135 – 2142.

[13] A. Neophytou, E. Mastorakos, R. S. Cant, The internal structure of igniting turbulent sprays as revealed by complex chemistry dns, Combustion and Flame 159 (2) (2012) 641 – 664.

[14] C. S. Yoo, T. Lu, J. H. Chen, C. K. Law, Direct numerical simulations of ignition of a lean n-heptane/air mixture with temperature inhomogeneities at constant volume: Parametric study, Combustion and Flame 158 (2011) 1727–1741.

[15] A. Krisman, E. R. Hawkes, M. Talei, A. Bhagatwala, J. H. Chen, A direct numerical simulation of cool- ame affected autoignition in diesel engine-relevant conditions, Proceedings of the Combustion Institute 36 (2017) 3567–3575.

[16] Z. Bouali, C. Pera, J. Reveillon, Numerical analysis of the influence of two-

phase flow mass and heat transfer on n-heptane autoignition, Combustion and flame 159 (6) (2012) 2056–2068.

[17] G. Borghesi, E. Mastorakos, Spontaneous ignition of isolated n-heptane droplets at low, intermediate, and high ambient temperatures from a mixture-fraction perspective, Combustion and Flame 162 (2015) 2544–2560.

[18] G. Borghesi, E. Mastorakos, Autoignition of n-decane droplets in the low-, intermediate-, and high-temperature regimes from a mixture fraction viewpoint, Flow, Turbulence and Combustion 96 (2016) 1107–1121.

[19] S. K. Aggarwal, A review of spray ignition phenomena: present status and future research, Prog. Energy Combust. Sci. 24 (2008) 565–600.

[20] H. Chiu, T. Liu, Group combustion of liquid droplets, Comb. Sci. Technol. 17 (1977) 127–131.

[21] H. Chiu, H. Kim, E. Croke, Internal group combustion of liquid droplets, in: T. combustion institute (Ed.), Proceedings of the nineteenth Symposium (International) on combustion, 1982.

[22] J. Reveillon, Multiphase reacting flows : modelling and simulation, edited by D.L. Marchisio and R. O. Fox, Springer, 2007, Ch. Direct numerical simulation of sprays: turbulent dispersion, evaporation and combustion.

[23] J. Reveillon, C. Péra, Z. Bouali, Examples of the potential of dns for the understanding of reactive multiphase flows, International Journal of Spray and Combustion Dynamics 3 (1) (2011) 63–92.

[24] S. Zhao, Z. Bouali, A. Mura, Computational investigation of weakly turbulent flame kernel growths in iso-octane droplet clouds in cvc conditions, Flow, Turbulence and Combustion 104 (1) (2020) 139–177.

[25] W. A. Sirignano, Fluid dynamics and transport of droplets and sprays, Cambridge university press, 2010.

[26] A. Patel, S. Kong, R. Reitz, Development and validation of a reduced reaction mechanism for HCCI engine simulations, SAE Paper 2004-01-0558 (2004).

[27] J. Reveillon, Numerical procedures to generate and visualize flow fields from analytical or experimental statistics: turbulent velocity, fluctuating scalars and variable density sprays, Journal of Flow Visualization and Image Processing 12 (3) (2005) 251–269.

[28] C. Crowe, M. Sommerfeld, Y. Tsuji (Eds.), Multiphase flows with droplets and particles, CRC Press, 1998.

[29] W. H. Press, S. A. Teukolsky, W. T. Vetterling, B. P. Flannery, Numerical Recipies, Cambridge University Press, 1992.

[30] J. Reveillon, F. Demoulin, Effects of the preferential segregation of droplets on evaporation and turbulent mixing, J. Fluid Mech. 583 (2007) 273–302.

[31] J. W. Gibbs, On the equilibrium of heterogeneous substances, Longmans, Green (1876).

[32] H. Pitsch, N. Peters., A consistent flamelet formulation for non-premixed combustion considering differential diffusion effects, Combustion and Flame 114 (1998) 26–40.

[33] R. Borghi, M. Champion, Modélisation et Théorie des Flammes, Editions Technip, 2000.

[34] R. Bilger, S. Starner, R. J. Kee, On reduced mechanisms for methane-air combustion in nonpremixed flames, Combustion and Flame 80 (1990) 135–149.

[35] J. Reveillon, L. Vervisch, Spray vaporization in nonpremixed turbulent combustion modeling : A single droplet model, Combustion and Flame 121 (2000) 75–90.

[36] S. Sreedharaa, K. Lakshmishaa, Direct numerical simulation of autoignition in a non-premixed, turbulent medium, Proceedings of the Combustion Institute 28 (1) (2000) 25–33.

[37] H. Im, J. Chen, C. Law, Ignition of hydrogen-air mixing layer in turbulent flows, Proceedings of the Combustion Institute 27 (1) (1998) 1047–1056.

[38] R. Hilbert, D. Thévenin, Autoignition of turbulent non-premixed flames investigated using direct numerical simulations, Combustion and Flame 128 (1-2) (2002) 22–37.